

# Time-correspondence differential ghost imaging

Ming-Fei Li, Yu-Ran Zhang, Kai-Hong Luo, Ling-An Wu,<sup>\*</sup> and Heng Fan<sup>†</sup>

*Laboratory of Optical Physics, Institute of Physics and Beijing National Laboratory for Condensed Matter Physics,  
Chinese Academy of Sciences, Beijing 100190, China*

(Dated: revised proof: Mar 12, 2013)

Experimental data with digital masks and a theoretical analysis are presented for an imaging scheme that we call time-correspondence differential ghost imaging (TCDGI). It is shown that by conditional averaging of the information from the reference detector but with the negative signals inverted, the quality of the reconstructed images is in general superior to all other ghost imaging (GI) methods to date. The advantages of both differential GI and time-correspondence GI are combined, plus less data manipulation and shorter computation time are required to obtain equivalent quality images under the same conditions. This TCDGI method offers a general approach applicable to all GI techniques, especially when objects with continuous gray tones are involved.

PACS numbers: 42.30.Va, 42.0.Ar, 42.50.St

Since the first “ghost image” was observed with entangled photon pairs generated by spontaneous parametric down-conversion [1], ghost imaging (GI) has become a focus of great attention as well as contention. In this technique, two spatially correlated beams are used to reconstruct the object image. The object beam passes through the object and its total intensity is collected by a “bucket” detector with no spatial resolution; a reference beam that does not interact with the object is measured by a pixel array detector. Various radiation sources may be employed, including quantum optical, pseudo-thermal [2], and true thermal light [3], while lensless configurations [4] and even systems using a computer generated thermal field with a single bucket detector [5, 6] have been demonstrated, stirring up a fundamental debate on whether GI is an intrinsically quantum phenomenon or whether it can be interpreted by classical optics [7–9]. This notwithstanding, GI displays great potential because it allows imaging of the object in harsh environments, e.g. in a scattering medium [10] or turbulent atmosphere [11–13], where standard imaging methods fail. Computational GI may also be used in optical encryption [14], and in ghost holography, where both intensity and phase information may be retrieved as well as in ghost holography, where both intensity and phase information may be retrieved [15]. The disadvantage is that very long measurement times are needed, while the visibility and signal-to-noise ratio (SNR) are low, especially with thermal light, which are serious drawbacks for practical applications. Although compressed sensing [16] can be used to reduce the number of measurements required for image reconstruction, or equivalently, greatly improve the image quality for the same number of exposures in GI, the corresponding data processing time is also greatly increased.

Recently, another method called differential ghost imaging (DGI) [17] was demonstrated which can dramatically enhance the SNR of conventional GI, but again with a huge amount of measurement data and more complex computation. Recently, Luo and co-workers *et al.* [18, 19] reported a technique that they called correspondence imaging (CI), in which a positive or negative image is retrieved by conditional averaging of the reference signals; that is, only those reference data that correspond to positive or negative intensity fluctuations of the bucket signal are selected for simple averaging, without the need to multiply by the bucket detector intensity itself. Compared with conventional GI for the same number of exposures, the processing time is greatly reduced, since, computationally, addition is faster than multiplication, whilst fewer frames are required to reconstruct the images. Moreover, the SNR of the negative image of CI is always better than that in conventional GI, but for the positive images it depends on the partition weighting [19].

In this paper we present another approach that we call time-correspondence differential ghost imaging (TCDGI), in which the advantages of DGI and CI are combined. Classical explanations of the phenomena are presented and we show that the image reconstructed by TCDGI can be as good as or even better than that of DGI, but with less data manipulation required and shorter computation times. This feature is a definite advantage and represents a step forward towards real practical applications.

The experimental setup, shown in Fig. 1, is a lensless GI system. A linearly polarized 632.8-nm He-Ne laser beam is projected onto a ground-glass disk rotating at 3 rad/min to produce a field of randomly varying speckles, which have an average diameter of  $\delta_0 \simeq 20 \mu\text{m}$ . This pseudo-thermal light is divided by a 50:50 beamsplitter (BS) into two spatially correlated object and reference beams; the former emerges from the object with an intensity distribution of  $I_B(\mathbf{x}_B)$  to be collected by the bucket detector  $D_B$ , while the latter ar-

<sup>\*</sup>Electronic address: wula@iphy.ac.cn

<sup>†</sup>Electronic address: hfan@iphy.ac.cn

rives at the reference detector  $D_R$  with a distribution of  $I_R(\mathbf{x}_R)$ , where  $\mathbf{x}$  is the transverse spatial coordinate and the suffixes B and R represent bucket and reference detectors, respectively. Both beams are collected by identical charge-coupled device (CCD) cameras (Imaging Source DMK 31BU03), of pixel size  $4.65 \mu\text{m}$ , which are synchronously triggered by a pulse generator. The area of the beams at the object and reference detector planes, which are at the same distance  $z_B = z_R = 215 \text{ mm}$  from the source, is  $A_{\text{beam}} \simeq 0.55 \text{ mm}^2$ , and contains  $N_{\text{speckle}} = A_{\text{beam}}/A_{\text{coh}} \simeq 1400$  speckles; where we have taken the coherence area to be  $A_{\text{coh}} \sim \delta_0^2$ .

In the experiment, both cameras captured  $1.4 \times 10^5$  frames with an exposure time of  $10^{-4} \text{ s}$ . A square region in each detector array, symmetric relative to the BS, of size  $160 \times 160$  pixels was selected, corresponding to the size of the object, which was a (virtual) digital mask. Two different masks of the same size were used, one with strong black-and-white contrast and the other with warm gray tones; their intensity transmission functions  $T_1(\mathbf{x})$  and  $T_2(\mathbf{x})$  are shown in Figs. 2(a) and 5(a), respectively. To obtain the bucket signal  $S_B$ , we multiply the matrix of the mask with the corresponding intensity values recorded by  $D_B$ , pixel by pixel, and then sum over all the intensities in the chosen region. As in CI [19], logical filtering is used to divide the reference signals  $I_R(\mathbf{x}_R)$  into subsets that satisfy specific conditions, and the image is then reconstructed by averaging over each subset separately, but here for TCDGI, the condition depends on the fluctuation of the differential signals.

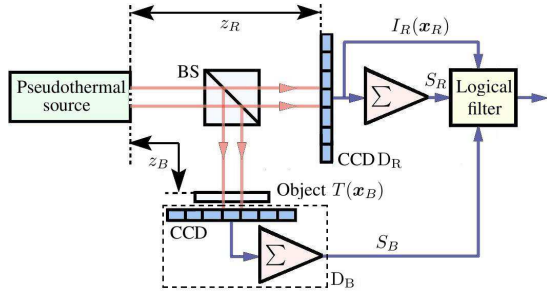


FIG. 1: (Color online) Schematic diagram of the experimental setup.

Our theory adopts a classical formalism in which the shot noise is neglected, and we simply set  $I_B(\mathbf{x}_B) = \alpha I_R(\mathbf{x}_R)$  where the factor  $\alpha$  exists because of the imbalance of the beamsplitter and detectors.

In conventional GI, the image in terms of  $T(\mathbf{x}_R)$  is obtained by the second-order correlation function of the intensity fluctuations of two detectors [2, 20]

$$\delta G_{GI}^{(2)}(\mathbf{x}_R) = \langle \delta S_B \delta I_R(\mathbf{x}_R) \rangle \simeq C_0 T(\mathbf{x}_R), \quad (1)$$

where  $C_0 = A_{\text{coh}} \langle I_R(\mathbf{x}_R) \rangle \langle I_B(\mathbf{x}_B) \rangle$  is a constant,  $T(\mathbf{x}_B)$  denotes the intensity transmission function of the object, and the bucket signal of the object arm is defined as  $S_B = \int I_B(\mathbf{x}_B) T(\mathbf{x}_B) d^2 \mathbf{x}_B$ ,  $\delta S_B = S_B - \langle S_B \rangle$ , and  $\delta I_R(\mathbf{x}_R) = I_R(\mathbf{x}_R) - \langle I_R(\mathbf{x}_R) \rangle$ .

To implement DGI [17], which can dramatically enhance the SNR, we need to define the integrated reference detector signal  $S_R = \int I_R(\mathbf{x}_R) d^2 \mathbf{x}_R$ . The differential bucket signal can be written in an operative form as  $S_\Delta = S_B - \frac{\langle S_B \rangle}{\langle S_R \rangle} S_R$ , and the quantity measured is

$$\delta G_{16}^{(2)}(\mathbf{x}_R) = \langle \delta S_\Delta \delta I_R(\mathbf{x}_R) \rangle \simeq C_0 \delta T(\mathbf{x}_R), \quad (2)$$

in which the fluctuating part is  $\delta T(\mathbf{x}_R) = T(\mathbf{x}_R) - \bar{T}$ , and  $\bar{T}$  can be expressed as  $\langle S_B \rangle / \alpha \langle S_R \rangle$ .

In the CI experiment [19], all the reference frames are divided into two subsets according to the sign of  $\delta S_B$ :

$$\{I_R(\mathbf{x}_R) | \delta S_B > 0\}, \{I_R(\mathbf{x}_R) | \delta S_B < 0\}. \quad (3)$$

From each of the subsets, the image is then reconstructed merely by simple averaging. We can obtain both positive and negative images from calculation of the conditional averages  $\langle I_R(\mathbf{x}_R) \rangle_+$  and  $\langle I_R(\mathbf{x}_R) \rangle_-$ , respectively, which can be written as

$$\begin{aligned} \langle I_R(\mathbf{x}_R) \rangle_\pm &\equiv \langle I_R(\mathbf{x}_R) \rangle + \langle \delta I_R(\mathbf{x}_R) \rangle_\pm \\ &\simeq \langle I_R(\mathbf{x}_R) \rangle + \langle \delta I_R(\mathbf{x}_R) (1 \pm \delta S_B / |\delta S_B|) \rangle \\ &\simeq \langle I_R(\mathbf{x}_R) \rangle \pm \langle \delta I_R(\mathbf{x}_R) \delta S_B \rangle / \langle |\delta S_B| \rangle \\ &\simeq \langle I_R(\mathbf{x}_R) \rangle \pm C_0 T(\mathbf{x}_R) / \langle |\delta S_B| \rangle, \end{aligned} \quad (4)$$

Here we have assumed that the positive and negative frames are approximately equal in number, and  $\langle A/B \rangle \simeq \langle A \rangle / \langle B \rangle$ , as in Ref. [21].

We now divide the reference CCD signals into two subsets according to the sign of  $\delta S_\Delta = S_\Delta - \langle S_\Delta \rangle = S_\Delta$ ,

$$\{I_R(\mathbf{x}_R) | \delta S_\Delta > 0\}, \{I_R(\mathbf{x}_R) | \delta S_\Delta < 0\}. \quad (5)$$

From Eqs. (2) and (4), we can thus obtain

$$\langle I_R(\mathbf{x}_R) \rangle_\pm^{diff} \simeq \langle I_R(\mathbf{x}_R) \rangle \pm C_0 \delta T(\mathbf{x}_R) / \langle |\delta S_\Delta| \rangle, \quad (6)$$

where  $\langle \dots \rangle_+^{diff}$  and  $\langle \dots \rangle_-^{diff}$  denote the averages of the positive and negative subsets, and correspond to the positive and negative images of TCDGI determined by the sign of  $\delta S_\Delta$ . In addition, it can be seen from Eqs. (4) and (6) that if we normalize the average of the conditional reference intensity after deducting the average of the reference signals, the image that we reconstruct by CI and TCDGI is almost the same as that in conventional GI and DGI. However, an even better way to reconstruct the image is to average all the normalized information from the reference detector but with the negative signals inverted:

$$\langle I_R(\mathbf{x}_R) \rangle_+^{diff} - \langle I_R(\mathbf{x}_R) \rangle_-^{diff} = \frac{2C_0 \delta T(\mathbf{x}_R)}{\langle |\delta S_\Delta| \rangle}, \quad (7)$$

where the image is retrieved by only averaging the reference data. Compared with DGI, the multiplication process is replaced by a logical filter process followed by simple addition, thus computing time is saved. Furthermore, TCDGI has a higher SNR than that of straightforward

CI, which means that, with the same amount of data, TCDGI gives a better image.

Next we discuss a more general scheme in which the selection condition is modified to:

$$\{I_R(\mathbf{x}_R)|\delta S_\Delta > k\}, \{I_R(\mathbf{x}_R)|\delta S_\Delta < -k\}, \quad (8)$$

where  $k$  is an intensity threshold satisfying  $0 \leq k \leq \max\{|\delta S_\Delta|\}$ . The averages of the reference signals that satisfy the threshold conditions are  $\langle I_R(\mathbf{x}_R) \rangle_{\pm k}^{diff} = \frac{1}{\beta} \left\langle I_R(\mathbf{x}_R) \left(1 \pm \frac{\delta S_B \mp k}{|\delta S_B \mp k|}\right) \right\rangle$ , where  $\beta = N_{k+}/N_{0+}$ , with  $N_{0+}$  and  $N_{k+}$  being, respectively, the number of frames satisfying  $\delta S_\Delta > 0$  and  $\delta S_\Delta > k$ , respectively. The expressions  $\langle \dots \rangle_{+k}^{diff}$  and  $\langle \dots \rangle_{-k}^{diff}$  denote the averages of the subsets selected by the above two threshold conditions, and  $\pm k^\pm$  means plus-or-minus the real number greater than  $+k$  (or less than  $-k$ ). Thus, a positive image can be obtained by subtracting these two averages:

$$\langle I_R(\mathbf{x}_R) \rangle_{+k}^{diff} - \langle I_R(\mathbf{x}_R) \rangle_{-k}^{diff} \simeq C_0 \delta T'(\mathbf{x}_R), \quad (9)$$

where  $\delta T'(\mathbf{x}_R) = \delta T(\mathbf{x}_R)/\beta|\delta S_\Delta - k|$ . In correlation imaging the main time consuming operation is the processing of all the big matrices of the reference frames, which is unavoidable even in DGI. In our TCDGI method, computation time is saved not just because we only use part of the matrices, but especially because we only need to add these matrices and then perform one minus operation, rather than having to multiply all of the differential bucket intensity signals one by one with the matching reference CCD matrix then take the average, as in the DGI protocol. Although the same original number of exposures frames must be taken and sorted, the sorting process can be regarded as almost instantaneous. For complex gray-scale objects, which we shall study below, much more imaging data is required, thus the advantage of less processing and computing time is even more pertinent.

We now present the experimental demonstrations of the above methods. In the first experiment, we used a digital mask which is a widely used standard in imaging processing [see Fig. 2(a)]. To compare the quality of the images obtained by different methods with the same standard, the gray scale of every image is normalized within the interval  $[0, 1]$ . This is achieved by subtracting the minimum element value from each matrix element of the image and then dividing the new matrix by the maximum element value. Figures 2(b) and 2(c) show the images retrieved after averaging over 140000 frames by DGI and GI, respectively (gray bars are provided for comparison on the right side of each row). In Fig. 2(d), we divide the reference frames into positive and negative subsets in accordance with the sign of  $\delta S_B$  in Eq. (3) as in CI and then obtain the image by subtracting the negative from the positive average,  $\langle I_R \rangle_+ - \langle I_R \rangle_-$ . Positive and negative images obtained by TCDGI, where instead of using  $\delta S_B$ , the sign of  $\delta S_\Delta$  is used to divide the reference signals, are shown in Figs. 2(e) and 2(f),

respectively; here 69600 frames were taken. Both positive and negative images are much better than in GI, although there are still blurred striations due to the rotation of the ground glass plate, which reflect the non-constant background  $\langle I_R(\mathbf{x}_R) \rangle$  in Eq. (4). If the number of frames is large enough, this term will tend to a constant, and the quality will improve. However, we can eliminate the background noise without increasing the number of measurements by directly subtracting the total average of the reference signals, to obtain  $\langle \delta I_R \rangle_+^{diff}$  and  $\langle \delta I_R \rangle_-^{diff}$ . As we can see from Figs. 2(g) and 2(h), the background has been almost completely eliminated, and both positive and negative images are much better and clearer than in all previous methods.

From Eq. (9) we can see that, in TCDGI, even if only part of the reference signals are chosen according to various threshold values, we can still retrieve relatively high quality images. Note that there is a one-to-one correspondence between the intensity threshold  $k$  and the number of selected frames; the latter decreases as  $k$  increases. The TCDGI images in the bottom row of Fig. 2 are reconstructed from different threshold values and frame numbers, again obtained by subtracting the negative from the positive image, see Eq. (9). Figures 2(i) to 2(l) are images retrieved for  $k_3 > k_2 > k_1 > k_0 = 0$  from 6000, 21 000, 31 500 and 69 600 frames, respectively, from each  $\delta S_\Delta > k_i$  and  $\delta S_\Delta < -k_i$  ( $i = 0, 1, 2, 3$ ) section. Although Fig. 2(i) does not appear to have such good contrast as in Fig. 2(l), it was reconstructed from only  $6000 \times 2$  frames as compared with  $69\,600 \times 2$ . On the other hand, the first smallest black square in the top left hand corner of the mask is quite visible in 2(i) but almost indiscernible in 2(l). In all cases, subtracting the negative frames always gives a greatly improved image, with much of the background noise removed.

To provide a quantitative comparison of the image quality obtained by various methods, we define the SNR [22, 23] as:

$$\text{SNR} = \frac{\text{Signal}}{\text{Noise}} = \frac{\sum_{i,j=1}^{M,N} [T_0(i,j) - \bar{T}_0]^2}{\sum_{i,j=1}^{M,N} [T(i,j) - T_0(i,j)]^2}, \quad (10)$$

where  $T_0(i,j)$  and  $T(i,j)$  are the transmission matrices of the object mask of size  $M \times N$  and the retrieved image, respectively, and  $\bar{T}_0 = (MN)^{-1} \sum_{i,j=1}^{M,N} T_0(i,j)$ . Generally speaking, we would expect the SNR to improve with the number of reference frames averaged over. The SNRs corresponding to  $k_3$ ,  $k_2$  and  $k_1$  in Figs. 2(i), 2(j) and 2(k) are 2.12, 3.21 and 3.24, respectively. But for a fair comparison, we should calculate the SNR for the same  $k$  value. In Fig. 3 we plot the SNR versus number of exposures for a threshold value of  $k = 0$ . We see that the SNR of DGI (stars) and TCDGI (crosses) are almost the same, and both are better than that of GI (circles), which is in good agreement with the results predicted by our theory. The highest points measured by DGI, GI and TCDGI correspond to the images in Figs. 2(b), 2(c) and 2(l), respectively.



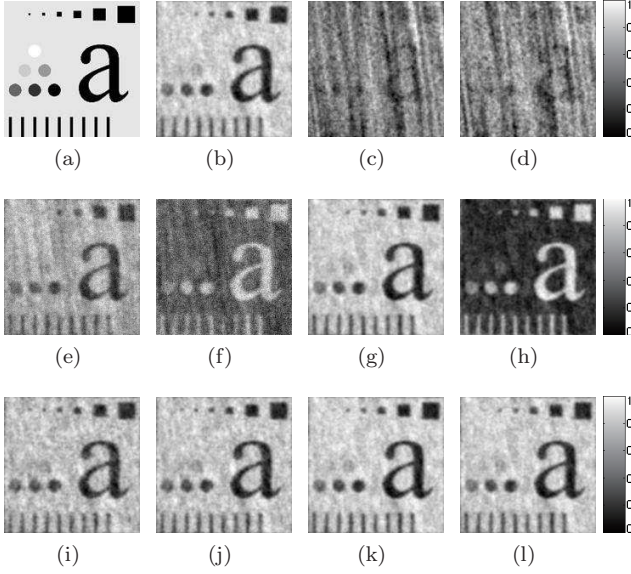


FIG. 2: Top row: (a) Digital mask 1. (b) DGI and (c) GI images, (d) CI positive minus negative image,  $\langle I_R \rangle_+ - \langle I_R \rangle_-$ , all from 140000 frames. Center row: (e) Positive TCDGI image  $\langle I_R \rangle_+^{diff}$ , (f) negative TCDGI image  $\langle I_R \rangle_-^{diff}$ , (g) positive TCDGI image minus reference signal average  $\langle \delta I_R \rangle_+^{diff}$ , (h) negative TCDGI image minus reference signal average  $\langle \delta I_R \rangle_-^{diff}$ , all from 69600 frames. Bottom row: TCDGI images obtained by  $\langle I_R \rangle_{k+}^{diff} - \langle I_R \rangle_{-k-}^{diff}$  with different thresholds. Number of frames averaged: (i)  $k_3$ ,  $6000 \times 2$ , (j)  $k_2$ ,  $21000 \times 2$ , (k)  $k_1$ ,  $31500 \times 2$ , (l)  $k_0 = 0$ ,  $69600 \times 2$ .

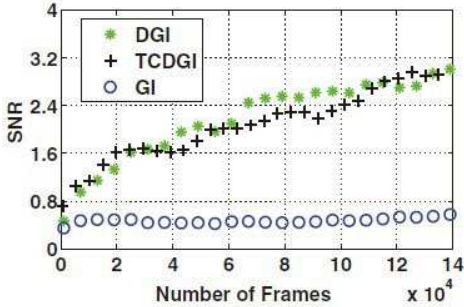


FIG. 3: (Color online) SNR vs. number of reference frames.

To demonstrate the advantages of TCDGI, the SNRs for different thresholds against the number of frames are given in Fig. 4. It is evident that as the threshold  $k$  increases, the SNR increases faster, but is limited by the number  $N_{k+}$  of reference frames available for averaging. As the computational time is approximately proportional to the number of frames, our TCDGI method is able to retrieve an image of better quality than DGI but with much less data manipulation and computing time. It is interesting that the SNR curves all exhibit some slight oscillations, as also observed in Ref. [15]. To our knowledge, this is partly due to experimental errors, and partly because the information in the CCD matrix frames is ac-

tually redundant for retrieving the object.

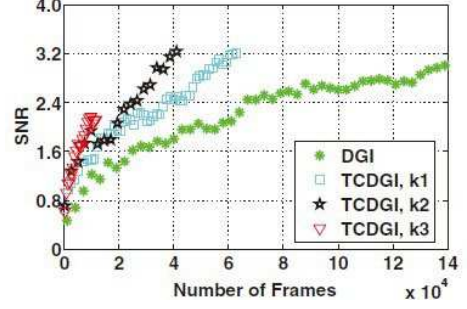


FIG. 4: (Color online) SNRs of DGI and TCDGI of different thresholds against the number of frames.

So far there are few GI experiments on objects with continuously changing gray tones, due to the immense number of exposures required. The mask that we used in the second experiment is the well-known photo of Lena that is widely used in traditional image processing tests. The images obtained by different methods are shown in Fig. 5, and their corresponding SNRs in the Table. We can see clearly that, for the same number of frames, the images retrieved by DGI (upper row) are inferior in quality to those retrieved by TCDGI (lower row). Moreover, with only 7600 exposures, we can still distinguish the TCDGI image in Fig. 5(g), while the DGI image from 8000 frames (Fig. 5(d)), is almost drowned in the noise. It is interesting that the maximum SNR value of 2.49, obtained by TCDGI, (1.95 for DGI) is not given by the highest number of exposures ( $69000 \times 2$  in Fig. 5(e), which has an SNR of 2.43) but by  $35400 \times 2$  exposures (Fig. 5(f)); the reason for this is, however, unclear at present, and deserves further analysis.

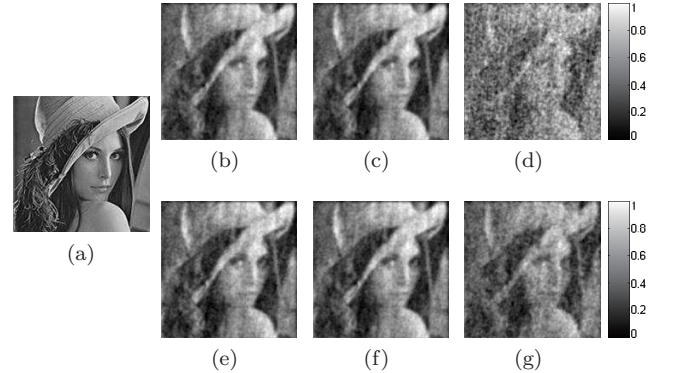


FIG. 5: (a) Digital mask of Lena. Upper row: DGI images from (b) 140000, (c) 71000, (d) 8000 frames. Lower row: TCDGI images from (e)  $69000 \times 2$ , (f)  $35400 \times 2$ , (g)  $3800 \times 2$  frames for  $k = 1, 2$  and  $3$ , respectively.

In conclusion, we have presented a new imaging technique called TCDGI by which we can retrieve the image of an object through conditional averaging of the spatial intensity together with inversion of the negative signals,

TABLE I: SNR of the images in Fig. 5.

Mask	DGI			TCDGI		
5(a)	5(b)	5(c)	5(d)	5(e)	5(f)	5(g)
$\infty^a$	2.10	1.95	0.75	2.43	2.49	1.65

<sup>a</sup>SNR of the mask is infinite, in accordance with Eq. (10).

using only the reference detector data. This method can dramatically enhance the SNR compared with conventional GI and CI, especially for objects with rich gray tones. Moreover, under the same conditions but with appropriate choice of threshold values, the retrieved image can be better than DGI, whilst being simpler to process, and requiring less data manipulation and computing

time. It is shown that the major contributions to the retrieved image come from the exposures with the largest intensity fluctuations. We believe that this new technique, which combines the advantages of CI and DGI, may become a standardized method in real applications where conventional imaging and GI protocols do not work well.

This work was supported by the National Basic Research Program of China (Grant No.2010CB922904), the National Natural Science Foundation of China (Grant No.60978002) and the Hi-Tech Research and Development Program of China (Grant No.2011AA120102). The authors are grateful for valuable discussions with Xue-Feng Liu and Xu-Ri Yao.

- 
- [1] T. B. Pittman, Y. H. Shih, D. V. Strekalov, and A. V. Sergienko, *Phys. Rev. A* **52**, R3429 (1995).
  - [2] A. Gatti, E. Brambilla, M. Bache, and L. A. Lugiato, *Phys. Rev. Lett.* **93**, 093602 (2004).
  - [3] D. Zhang, Y. H. Zhai, L. A. Wu, and X. H. Chen, *Opt. Lett.* **30** 2354 (2005).
  - [4] A. Valencia, G. Scarcelli, M. D'Angelo, and Y. H. Shih, *Phys. Rev. Lett.* **94**, 063601 (2005).
  - [5] J. H. Shapiro, *Phys. Rev. A* **78**, 061802(R) (2008).
  - [6] Y. Bromberg, O. Katz, and Y. Silberberg, *Phys. Rev. A* **79**, 053840 (2009).
  - [7] R. S. Bennink, S. J. Bentley, and R. W. Boyd, *Phys. Rev. Lett.* **89** 113601 (2002).
  - [8] Y. H. Shih, *Quantum Inf. Process.* **11**, 995 (2012).
  - [9] J. H. Shapiro, R. W. Boyd, *Quantum Inf. Process.* **11**, 1003 (2012).
  - [10] W. L. Gong, S. S. Han, *Opt. Lett.* **36**, 394 (2011).
  - [11] J. Cheng, *Opt. Exp.* **17**, 7916-7921 (2009).
  - [12] P. L. Zhang, W. L. Gong, X. Shen, and S. S. Han, *Phys. Rev. A* **82**, 033817 (2010).
  - [13] R. E. Meyers, K. S. Deacon, and Y. H. Shih, *Appl. Phys. Lett.* **98**, 111115 (2011).
  - [14] P. Clemente, V. Durn, V. Torres-Company, E. Tajahuerce, and J. Lancis, *Opt. Lett.* **35**, 2391 (2010).
  - [15] P. Clemente, V. Durn, V. Torres-Company, E. Tajahuerce, and J. Lancis, *Phys. Rev. A* **86**, 041803(R) (2012).
  - [16] O. Katz, Y. Bromberg, and Y. Silberberg, *Appl. Phys. Lett.* **95**, 131110 (2009).
  - [17] F. Ferri, D. Magatti, L. A. Lugiato, and A. Gatti, *Phys. Rev. Lett.* **104**, 253603 (2010).
  - [18] L. A. Wu, K. H. Luo, *AIP Conf. Proc.* **1384**, 223 (2011).
  - [19] K. H. Luo, B. Q. Huang, W. M. Zheng, and L. A. Wu, *Chin. Phys. Lett.* **29**, 074216 (2012).
  - [20] F. Ferri, D. Magatti, V. G. Sala, and A. Gatti, *Appl. Phys. Lett.* **92**, 261109 (2008).
  - [21] B. Q. Sun, S. Welsh, M. Edgar, J. Shapiro, and M. Padgett, *Opt. Express* **20**, 16892 (2012).
  - [22] K. R. Castleman, *Digital Image Processing*, (Prentice Hall Press, Upper Saddle River, New Jersey, USA, 1996).
  - [23] J. C. Russ, *The image processing handbook*, Sixth Edition (CRC Press, Boca Raton, FL, USA, 2011).